Monthly Notices
of the
ROYAL ASTRONOMICAL SOCIETY

MNRAS **452,** 1717–1726 (2015) doi:10.1093/mnras/stv1385

Outwards migration for planets in stellar irradiated 3D discs

E. Lega,[1⋆] A. Morbidelli,[1⋆] B. Bitsch,[2] A. Crida[1] and J. Szulágyi[1]

[1] *Université Nice Sophia Antipolis, CNRS UMR 7293, Observatoire de la Côte d'Azur, Bv. de l'Observatoire, CS 34229, F-06304 Nice cedex 4, France*
[2] *Lund Observatory, Department of Astronomy and Theoretical Physics, Lund University, SE-22100 Lund, Sweden*

Accepted 2015 June 19. Received 2015 June 18; in original form 2015 March 31

ABSTRACT

For the very first time we present 3D simulations of planets embedded in stellar irradiated discs. It is well known that thermal effects could reverse the direction of planetary migration from inwards to outwards, potentially saving planets in the inner, optically thick parts of the protoplanetary disc. When considering stellar irradiation in addition to viscous friction as a source of heating, the outer disc changes from a shadowed to a flared structure. Using a suited analytical formula it has been shown that in the flared part of the disc the migration is inwards; planets can migrate outwards only in shadowed regions of the disc, because the radial gradient of entropy is stronger there. In order to confirm this result numerically, we have computed the total torque acting on planets held on fixed orbits embedded in stellar irradiated 3D discs using the hydrodynamical code FARGOCA. We find qualitatively good agreement between the total torque obtained with numerical simulations and the one predicted by the analytical formula. For large masses ($>20\,M_\oplus$) we find quantitative agreement, and we obtain outwards migration regions for planets up to $60\,M_\oplus$ in the early stages of accretional discs. We find nevertheless that the agreement with the analytic formula is quite fortuitous because the formula underestimates the size of the horseshoe region; this error is compensated by imperfect estimates of other terms, most likely the cooling rate and the saturation.

Key words: methods: numerical – planet–disc interactions – protoplanetary discs.

1 INTRODUCTION

In recent years, it has been shown that low-mass planets ($[5, 20]\,M_\oplus$) can migrate outwards in discs with non-isothermal effects (Paardekooper & Mellema 2006; Baruteau & Masset 2008; Kley & Crida 2008; Kley, Bitsch & Klahr 2009; Masset & Casoli 2009, 2010; Paardekooper et al. 2010; Paardekooper, Baruteau & Kley 2011; Lega et al. 2014). Precisely, the migration in the inner part of a radiative disc can be directed outwards, while it remains directed inwards in the outer disc (Bitsch & Kley 2011). This establishes the existence of a critical radius where migration vanishes, towards which planetary cores migrate from both the inner and the outer part of the disc. Therefore, the zero migration location acts as a planet trap at which proto-planets can accumulate in resonances, collide and eventually form bigger objects (Lyra, Paardekooper & Mac Low 2010; Cossou et al. 2014; Coleman & Nelson 2014).

In all these works the heating is provided by viscous friction and the cooling by radiative diffusion (in 3D discs) or by a local cooling rate (in 2D discs). More recently, Bitsch et al. (2013) have shown the importance of stellar irradiation on the disc structure and the consequences for planetary migration. The main result is that when considering stellar irradiation the outer disc changes from a shadowed to a flared disc. Nonetheless, opacity transitions (e.g. the iceline) create bumps in the aspect ratio and hence shadowed regions. In the flared part of the disc the migration turns out to be inwards and planets can migrate outwards only in shadowed regions of the disc, where the radial gradient of entropy is much steeper than in the flared part of the disc. These results were obtained in equilibrium discs with uniform viscosity featuring a zero radial mass flux (Bitsch et al. 2013) and extended to the case of accretion discs with an alpha prescription for the viscosity (Shakura & Sunyaev 1973) in Bitsch et al. (2014). This second case is of particular interest, since a given mass-flow ($\dot{M}$) rate corresponds to a specific disc age (Hartmann et al. 1998) so that investigating the disc structure for different values of $\dot{M}$ is equivalent to studying the disc structure as a function of the disc evolution (Bitsch et al. 2014, 2015).

In Bitsch et al. (2013, 2014, 2015) the planet migration maps have been obtained applying the torque formula of Paardekooper et al. (2011) using the disc properties obtained in the simulations. The formula, although very complex, is based on the fact that the torque exerted by the protoplanetary disc on to the planet has two main contributions: (i) the so-called Lindblad torque due to the spiral arms launched by the planet in the disc, which is not affected by the

⋆E-mail: elena@oca.eu (EL); morby@oca.eu (AM)

equation of state,[1] and (ii) the co-orbital corotation torque caused by material librating in the horseshoe region. When considering radiative effects the corotation torque contribution can be positive and possibly dominate over the negative Lindblad torque, leading to outwards migration. The Paardekooper et al. formula was calibrated with a 2D hydrodynamical model for low-mass planets ($5\,M_\oplus$).

With a specific disc setting not accounting for stellar irradiation, Kley et al. (2009) found positive total torque for planetary masses in the range [5, 30] Earth masses. The influence of the disc's mass on the migration was studied in Bitsch & Kley (2011) and its application to Earth sized planets was addressed by Lega et al. (2014) who found the contribution of a new torque not accounted for by the formula. This new negative torque is due to the formation of an asymmetric cold and dense finger of gas driven by circulation and libration streamlines.

The aim of this paper is to investigate numerically the total torque acting on planets kept on fixed orbits in 3D stellar irradiated discs and provide quantitative comparisons with the Paardekooper et al. (2011) formula. We use the explicit/implicit hydrodynamical code FARGOCA (Lega et al. 2014) that includes a two-temperature solver for radiative transfer in the flux-limited approximation.

In principle, stellar heating only changes the structure of the disc and does not act on the mechanism responsible for outwards migration directly. Nevertheless, the analytical formula has been calibrated on 2D discs so that a quantitative test on the validity of that formula for realistic 3D discs is needed. Moreover, a constant mass flow $\dot{M}$ through the disc (Bitsch et al. 2014) might have an influence on the torque acting on planets and, to our knowledge, this case has never been tested before in 3D discs with a non-isothermal EOS.

The paper is organized as follows: the physical modelling is presented in Section 2; in Section 3 we describe the migration maps obtained from the analytic formula applied to our 2D unperturbed discs.[2] In Sections 4 and 5 we provide results of 3D simulations done, respectively, on a constant viscosity stellar irradiated equilibrium disc and on an α-viscosity accretion disc. In Section 6 we go beyond the simple comparisons of the net torques predicted analytically and measured numerically, focusing on a key ingredient of the analytic formula: the size of the corotation zone, which governs the corotation torque and the torque saturation. The conclusions are provided in Section 7.

2 PHYSICAL MODELLING

The protoplanetary disc is treated as a 3D non-self-gravitating gas whose motion is described by the Navier–Stokes equations. We use spherical coordinates (r, θ, φ) where r is the radial distance from the star, i.e. from the origin, θ is the polar angle measured from the z-axis (the colatitude) and φ is the azimuthal coordinate starting from the x-axis. The mid-plane of the disc is at the equator $\theta = \frac{\pi}{2}$. We work in a coordinate system which rotates with angular velocity:

$$\Omega_\mathrm{p} = \sqrt{\frac{G(M_\star + m_\mathrm{p})}{{a_\mathrm{p}}^3}} \simeq \sqrt{\frac{GM_\star}{{a_\mathrm{p}}^3}},$$

where $M_\star$ is the mass of the central star, G is the gravitational constant and a_p is the semi-major axis of a planet of mass m_p, assumed to be on a circular orbit. The gravitational influence of the planet on the disc is modelled as in Kley et al. (2009) using a cubic-potential of the form:

$$\Phi_\mathrm{p} = \begin{cases} -\frac{m_\mathrm{p} G}{d} & d > \epsilon \\ -\frac{m_\mathrm{p} G}{d} f(\frac{d}{\epsilon}) & d \leq \epsilon, \end{cases} \quad (1)$$

where d is the distance from the disc element to the planet and ϵ is the softening length. Writing $x = d/\epsilon$ the function f is given by

$$f(x) = x^4 - 2x^3 + 2x.$$

We have considered $\epsilon = 0.6 R_\mathrm{H}$ in our simulations sets SED and SAD and $\epsilon = 0.5 R_\mathrm{H}$ for simulation set RED, with R_H the Hill radius of the planet:

$$R_\mathrm{H} = a_\mathrm{p} \sqrt[3]{\frac{m_\mathrm{p}}{3M_*}}.$$

We will discuss in Section 6 the dependence of the total torque on the softening length.

In the Paardekooper formula, there is also a softening length parameter β and it has been fixed to $\beta = 0.35H$ (H being the disc's local scale height) from previous comparison between the formula and 3D simulations (Bitsch & Kley 2011).

The hydrodynamical equations solved in the code are described in Lega et al. (2014), the two-temperature approach for the stellar irradiation was described in detail in Bitsch et al. (2013) and the opacity prescription in Bitsch et al. (2014). The flux received from the star at a radial distance r is

$$F_\star = R_\star^2 \sigma T_\star^4 / r^2, \quad (2)$$

where the radius of the star is set to $R_\star = 1.5\,R_\odot$ and the temperature $T_\star = 4370\,\mathrm{K}$ (appropriate for a solar-type protostar). We consider the disc settings of Bitsch et al. (2013), namely a disc extending from $r_\mathrm{min} \leq r \leq r_\mathrm{max}$ with $r_\mathrm{min} = 1\,\mathrm{au}$ and $r_\mathrm{max} = 50\,\mathrm{au}$. In the vertical direction the disc extends from the mid-plane ($\theta \simeq 90^\circ$) to 20° above the mid-plane, i.e. $\theta \simeq 70^\circ$. The initial surface density profile is $\Sigma(r) = \Sigma_0 (r/a_\mathrm{J})^{-b}$ and $a_\mathrm{J} = 5.2\,\mathrm{au}$.

We consider in the following different sets of simulations. Precisely, we consider a stellar irradiated equilibrium disc (set SED hereafter), with uniform viscosity (viscosity coefficient $\nu = 10^{-5} a_\mathrm{J}^2 \Omega_\mathrm{p}$), $\Sigma_0 = 4.88 \times 10^{-4}$ in code units ($147\,\mathrm{g\,cm^{-2}}$) and $b = 0.5$. We also consider a stellar irradiated accretion discs (set SAD hereafter) with alpha viscosity ($\alpha = 0.0054$), constant $\dot{M} = 4 \times 10^{-8}\,M_\odot\,\mathrm{yr}^{-1}$ and initial value of $b = 15/14$ and of $\Sigma_0 = 430\,\mathrm{g\,cm^{-2}}$. The initial value of b corresponds to the radial surface density profile in flared disc[3] with constant $\dot{M}$ at all orbital distances. A disc with $\dot{M} = 4 \times 10^{-8}\,M_\odot\,\mathrm{yr}^{-1}$ corresponds to the early evolution stages of accretion discs and is probably younger than 1 Myr (Hartmann et al. 1998). The disc structure of the SAD case is discussed in Bitsch et al. (2015).

For comparison, we will also consider the case of a radiative equilibrium disc (RED) with uniform viscosity ($\nu = 10^{-5} a_\mathrm{J}^2 \Omega_\mathrm{p}$) and $b = 0.5$, where the only source of heating is viscous heating (set RED hereafter). This setup of the RED disc has been previously studied in Kley et al. (2009); Bitsch & Kley (2011) and in Lega et al. (2014) for planetary masses up to $30\,M_\oplus$.

Before placing the planet in a 3D disc, we bring the disc to radiative equilibrium. We first model each disc in 2D, with coordinates (r, θ). For the accretion disc the (r, θ) disc evolution is explained in detail in Bitsch et al. (2014, 2015). Once the 2D equilibrium is

[1] Actually, it scales with $\gamma\Gamma_0$, with Γ_0 given in equation (5).
[2] Discs in thermal equilibrium in the $(r - z)$ plane.
[3] With flaring index 2/7.

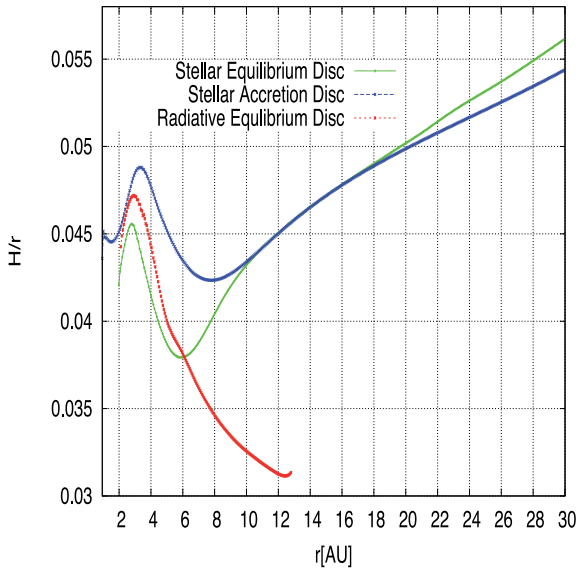

Figure 1. Aspect ratio of the 2D (r, θ) equilibrium of simulation set SED (green) and SAD with $\dot{M} = 4 \times 10^{-8}$ (blue). For comparison the red curve provides the aspect ratio of the RED studied in Kley et al. (2009) and Lega et al. (2014).

achieved all the gas fields are expanded to 3D. The aspect ratio of the 2D equilibrium for the SED, the SAD with $\dot{M} = 4 \times 10^{-8}\,\mathrm{M}_\odot\,\mathrm{yr}^{-1}$ and the RED are reported in Fig. 1. We remark that for the SED and RED with uniform viscosity, the settling of the aspect ratio to an equilibrium value does not change the surface radial density profile of the disc. Instead, in the SAD disc, in which the viscosity follows the alpha-prescription and thus depends on the disc's local scale height H, the resulting surface density profile at equilibrium is somewhat different from the initial one (see Bitsch et al. 2014).

In the two cases where the disc is heated by the star we observe the typical profile of a flared disc, while we have a shadowed disc in the RED case. The bump in H/r around 3–4 au is caused by a transition in opacity that changes the local cooling rate of the disc and hence changes the disc's temperature (Bitsch et al. 2014).

The resolution of our computational grid is chosen in order to have in the radial direction approximatively n grid cells in the horseshoe region. The half-width of the planet's horseshoe region is given in the isothermal disc approximation (Masset, D'Angelo & Kley 2006) by

$$x_{\mathrm{hs2D}} = 1.16 a_\mathrm{p} \sqrt{\frac{q}{h}}\,, \tag{3}$$

where $q = m_\mathrm{p}/M_\star$ and h is the disc aspect ratio at a_p. We have checked that this formula can still be used as a guideline for the choice of the resolution for non-isothermal 3D discs with and without stellar irradiation. However, equation (3) is based on the equivalence of the linear corotation torque and the horseshoe drag in 2D discs. In Masset et al. (2006) it has been shown that non-linearities appear on the flow for mass ratios $q \geq h^3$. For these planetary masses the horseshoe region is larger than the linear prediction resulting in a boost of the corotation torque. It is therefore important to check whether also in 3D hydrodynamical simulations the horseshoe width increases for $q \geq h^3$ and what is the corresponding impact in the corotation torque. Section 6 is devoted to this topic.

The values of the masses and resolutions $(N_r, N_\theta, N_\varphi)$ for the SED disc are shown in Table 1. In Lega et al. (2014) we have shown

Table 1. Simulations parameters for set SED. Embedded planets are at distance 4 au from the star.

Mass ($\mathrm{M}_\oplus$)	(N_r,N_θ, N_φ)	n cells in x_{hs2D}
8	(1326, 66, 908)	4
10	(1186, 66, 812)	4
20	(1086, 82, 740)	5
25	(1010, 66, 702)	4
25	(1238, 80, 876)	5
30	(911, 66, 620)	4
40	(770, 66, 542)	4
50	(670, 60, 468)	4
60	(612, 60, 430)	4
60	(764, 66, 540)	5

that a resolution of four grid cells in the half-width of the horseshoe region matched the requirement of having resolution-independent results within reasonable CPU times for masses up to $20\,\mathrm{M}_\oplus$. Here we use four grid cells in the half-width of the horseshoe region also for planets with masses larger than $20\,\mathrm{M}_\oplus$; We have tested that results are stable when increasing the resolution to five grid cells in some test cases.

Concerning the calculation of the gravitational torque acting on the planet we recall that it is common to exclude the inner part of the Hill sphere of the planet. This is obtained by applying a tapering function (named Hill cut in the following) which in our case reads (Kley et al. 2009):

$$f_b(d) = \left[\exp\left(-\frac{d/R_\mathrm{H} - b}{b/10}\right) + 1\right]^{-1}. \tag{4}$$

The value of f_b is zero at the planet location and increases to 1 at distances d from the planet larger than the Hill radius R_H. The parameter b denotes the distance from the planet, in unit of Hill radius, at which $f_b = 1/2$. Here we use $b = 0.8$ (Crida et al. 2009).

This procedure allows us to exclude the part of the disc that is gravitationally bound to planets that form a circum-planetary disc. However, this prescription is not justified for small mass planets that do not have a circum-planetary disc. For small planets we mean planets having a Bondi radius (R_B) smaller than their Hill radius. From the definition of the Bondi and Hill radii one obtains $R_\mathrm{B} < R_\mathrm{H}$ for $q < h^3/\sqrt{3}$.[4] In the following we show the total torque computed with Hill cut, and, for planetary masses satisfying $q < h^3/\sqrt{3}$, we also show the total torque computed without Hill cut.

3 MIGRATION MAPS

The change in the disc structure due to stellar irradiation has important consequences for the migration of embedded bodies (Bitsch et al. 2013). One can estimate the torque acting on planets using the formula provided by Paardekooper et al. (2011). The migration maps obtained from the formula are shown in Fig. 2 for respectively set SED (top panel), set SAD with $\dot{M} = 4 \times 10^{-8}\,\mathrm{M}_\odot\,\mathrm{yr}^{-1}$ (middle panel) and set RED (bottom panel). The values of the total torque Γ_tot are normalized with respect to

$$\Gamma_0 = (q/h)^2 \Sigma_\mathrm{p} a_\mathrm{p}^4 \Omega_\mathrm{p}^2 \tag{5}$$

where Σ_p is the disc's surface density at the planet location a_p.

[4] We notice that the parameter that determines the flow linearity in the planet vicinity is $q < h^3$ (Masset et al. 2006).

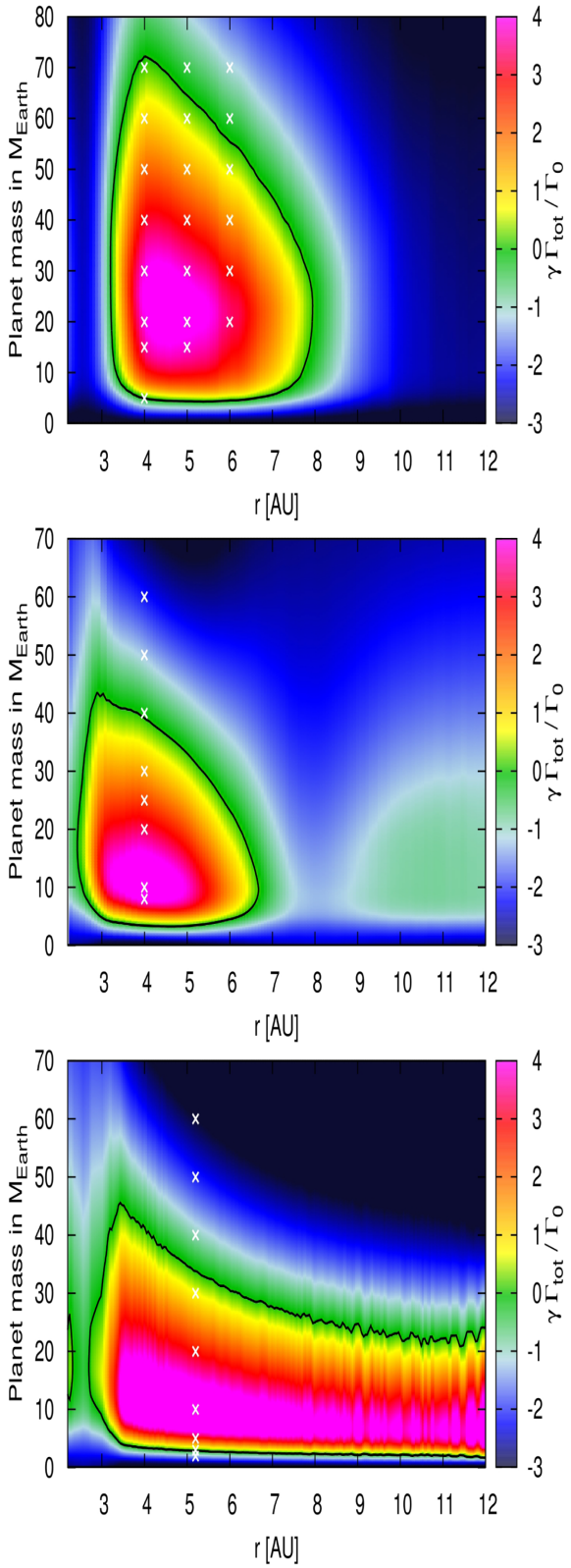

Figure 2. Migration maps for simulation set SAD with $\dot{M} = 4 \times 10^{-8}\,M_\odot\,yr^{-1}$ (top), SED (middle). For comparison, the migration map of the RED is also plotted (bottom). The white x symbols indicate the position and the masses of the planets for which we compute the total torque with 3D simulations in this paper.

We do not enter here the details of the torque formula provided by Paardekooper et al. (2011), we just recall that outwards migration is a delicate process depending on the dynamical properties of the corotation region as well as on the viscosity of the disc and of its cooling properties. Different time-scales are at play (see Bitsch & Kley 2010), in order to detect a positive corotation torque contribution which possibly dominates over the negative Lindblad torque.

We remark that the formula has been obtained for planets that do not perturb the disc significantly ($q < h^3$, i.e. linear regime) while the maps shown in Fig. 2 consider also intermediate-mass planets (30–70 $M_\oplus$). The torque saturation, which determines the upper limit in planet mass for outwards migration, depends on the viscous time-scale defined by

$$\tau_\nu = (x_{\rm hs2D}\gamma^{-1/4})^2/\nu, \tag{6}$$

where γ is the adiabatic index, $\gamma = 1.4$ in our simulations. The width of the horseshoe region is $x_{\rm hs2D}/\gamma^{1/4}$ in order to take adiabatic effects into account (Paardekooper & Papaloizou 2009). However, for intermediate-mass planets, the actual width of the horseshoe region can be different from $x_{\rm hs2D}$ of equation (3) (Masset et al. 2006) and this difference can have an impact on torque saturation.

In the migration map of the SAD case (Fig. 2,top) we see that, using $x_{\rm hs2D}/\gamma^{1/4}$, torque saturation is supposed to occur for quite large planetary masses and outwards migration is expected for planets up to 70 $M_\oplus$ (this upper limit can moderately change by changing the smoothing length β.).

It is interesting to check this result with 3D numerical simulations, because outward migration of intermediate-mass planets has important impacts for formation models of giant planets. In fact, giant planet precursors could be prevented from migrating into the inner disc before they reach a mass that allows gap opening and therefore slower inward migration in the type-II migration regime.

In order to test the validity of the formula we have considered planets of different masses held on fixed orbits in each of the three considered discs and we have computed the evolution of the torque with time until we obtain a stationary state. We choose the distance of the planets from the star within the region of expected outwards migration from Fig. 2.

4 EQUILIBRIUM DISCS

In the SED we have embedded planets of different masses held on a fixed orbit at $r = 4$ au, for which we expect outwards migration from the torque formula (Fig. 2, middle panel). Let us notice that, in the inner part of the disc, the aspect ratio of the SED is very similar to that of the RED (Fig. 1); since the density gradient is the same for both discs the computation of the total torque should give results similar to those obtained in Kley et al. (2009) and Lega et al. (2014).

When considering planets at 4 au we observe (Fig. 3) that for masses larger than 30 Earth masses the torque is slightly larger than the one provided by the formula and the transition to negative torque occurs at 45 $M_\oplus$ instead of 40 $M_\oplus$ as expected from the formula (Fig. 2, middle panel). However, the overall picture is quite in good agreement with the results provided by the analytical formula. For comparison we have extended our previous study of the RED from Lega et al. (2014) for planets at 5.2 au towards planets with masses up to 60 Earth masses. We can appreciate in Fig. 4 the agreement between the results of numerical simulations and the values given by the analytical formula.

In both the RED and SED, we provide in the following subsections a quantitative comparison between the values of the torque

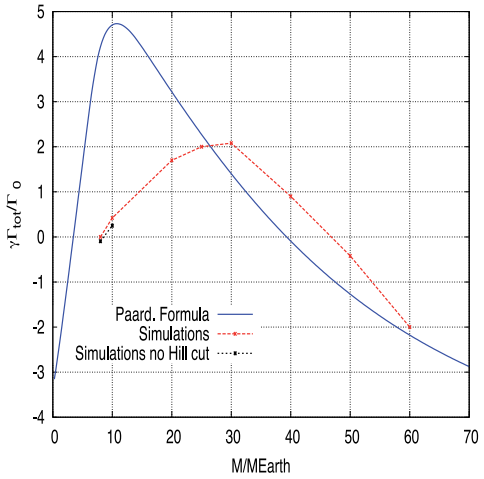

Figure 3. Stellar irradiated equilibrium disc (SED): comparison with Paardekooper et al. (2011) formula for planets on fixed orbits at 4 au. For planets of 10 and 8 $M_\oplus$ we also show the value of the torque computed without the Hill cut (see text).

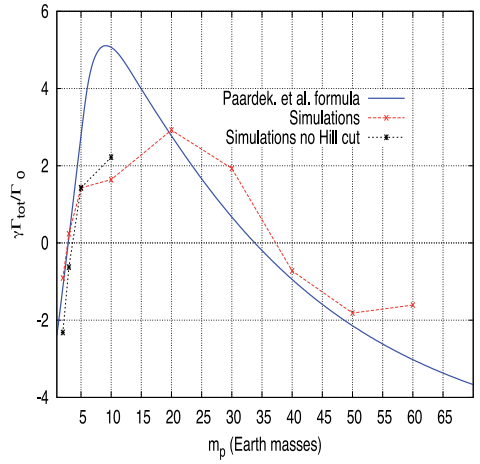

Figure 4. Same as Fig. 3 for the radiative disc (RED) studied in Lega et al. (2014) whose aspect ratio is reported in Fig. 1 and the corresponding migration map in Fig. 2 (bottom panel). For planet of mass smaller than 10 $M_\oplus$ we also show the value of the torque computed without the Hill cut (see text).

resulting from numerical simulations and the values given by the formula.

4.1 Planetary masses smaller than 10 $M_\oplus$

In the case of the SED disc, the minimum planetary mass to have outwards migration is somewhat larger than that predicted in the Paardekooper et al. (2011) formula (about 8 $M_\oplus$ against 4 $M_\oplus$). This minimum mass is very important for giant planet formation models. The larger transition mass that we find can be explained with the cold finger effect studied in Lega et al. (2014). The unperturbed temperature at the planet location is of 112 K, and, according to the criterion given in Lega et al. (2014), a negative contribution to the total torque (cold finger) exists when the Bondi radius R_B is smaller that the Hill radius R_H. We have suggested

$$\frac{R_B}{R_H} = \frac{(m_p/7.1 M_\oplus)^{2/3}}{(a/5.2\,\mathrm{au})(T/75\,\mathrm{K})}. \quad (7)$$

Applying equation (7) for planets at 4 au where $T = 112$ K, we obtain $\frac{R_B}{R_H} = 1$ for a 10 $M_\oplus$ and $\frac{R_B}{R_H} = 0.6$ for a 5 $M_\oplus$ planet. Thus, the expected transition between outwards and inwards migration occurs in the interval [5, 10] $M_\oplus$ in very good agreement with the value of 8 $M_\oplus$ found in the simulations. In the RED disc, the minimum planetary mass to have outwards migration is about 4 $M_\oplus$ against 2 $M_\oplus$, due to the cold finger effect found in Lega et al. (2014).

4.2 Planetary masses in the interval 10-30 $M_\oplus$

In Fig. 4 we notice that the maximum value of the computed torque as a function of planetary mass is about a factor of 2 smaller than the maximum provided by the formula. The planetary mass for which we measure the largest positive torque value is respectively of 20 $M_\oplus$ for the RED case and of 30 $M_\oplus$ for the SED case. In both cases the formula provides the largest positive torque for a planet of 10 $M_\oplus$, and the onset of saturation occurs at planetary masses smaller than what found in 3D simulations. We will discuss this point in Section 6. These quantitative discrepancies have already been pointed out by Kley et al. (2009) caused by differences between 2D and 3D effects.

4.3 Planetary masses larger than 30 $M_\oplus$

The analytical formula was derived for small mass planets (5 $M_\oplus$), i.e. for planets that only slightly perturb the disc. However, larger mass planets start opening a partial gap in the disc, meaning they significantly perturb the disc. These perturbations make the application of the torque formula dubious for masses larger than 30 $M_\oplus$. However, the density in the corotation region is perturbed by less than 30 per cent up to 60 $M_\oplus$, i.e. we are still far from planetary masses which really open a gap in the disc.

We remark that the formula and simulation results are in very good agreement for masses larger than 30 $M_\oplus$. The torques in the formula are calculated from the gradients of surface density, temperature and entropy in the unperturbed disc. In the formula, the corotation torque saturates as the planet mass increases, making the total torque transit to negative. In our simulations, the total torque is obtained directly from the density structure of the disc, meaning that on top of saturation effects, the partial opening of a gap is also taken into account, decreasing even more the corotation torque. The fact that these two different approaches match in the total torque may be a coincidence, but we remind that the density in the corotation region is perturbed by less than 30 per cent up to 60 $M_\oplus$.

We can conclude this section saying that when we take into account stellar irradiation in an equilibrium disc no additional effects on the total torque acting on planets in the explored mass range of [8, 60] Earth masses are observed. Moreover, the analytical formula Paardekooper et al. (2011) can be used with good confidence when performing, for example, *N*-body simulations with a migration prescription.

5 STELLAR IRRADIATED ACCRETION DISCS

Protoplanetary discs accrete gas on to the central Star (Lynden-Bell & Pringle 1974). Thus equilibrium discs like the SED and RED cases investigated above are not a good approximation of reality,

Table 2. Simulation parameters for set SAD.

Mass ($M_\oplus$)	$(N_r, N_\theta, N_\varphi)$	n cells in x_{hs2D}	Distance (au)
5	(1600, 110, 1132)	4	4
15	(1320, 96, 910)	4	4
15	(1256, 90, 886)	6	5
20	(1066, 74, 750)	4	4
20	(1600, 100, 1132)	7	4
20	(1318, 80, 920)	6	5
20	(1528, 90, 1072)	7	5
20	(1134, 90, 758)	7	6
30	(1502, 90, 1068)	7	4
30	(1250, 76, 878)	7	5
30	(1080, 78, 718)	7	6
40	(1360, 86, 972)	7	4
40	(1080, 70, 758)	7	5
40	(926, 66, 622)	7	6
50	(1226, 76, 868)	7	4
50	(966, 70, 680)	7	5
50	(826, 66, 558)	7	6
60	(1118, 80, 794)	7	4
60	(882, 66, 624)	7	5
60	(754, 66, 514)	7	6
70	(1034, 74, 730)	7	4
70	(808, 66, 576)	7	5
70	(692, 56, 476)	7	6

given that they do not transport mass radially. A much better approximation are the discs where the mass flow $\dot{M}$ is independent of radius, called accretion discs. Their structure has been investigated in Bitsch et al. (2014). Here we check the validity of the Paardekooper et al. (2011) formula in these more realistic discs.

We consider the case of an accretion disc with constant $\dot{M} = 4 \times 10^{-8}\,M_\odot\,yr^{-1}$ and we compute the total torque for planets in the mass interval 20–70 Earth masses placed at distances of 4 au, 5 au and 6 au from the central star. We have also made a few tests on smaller planetary masses. The values of the masses and resolutions $(N_r, N_\theta, N_\varphi)$ for the SAD disc are shown in Table 2.

We have used a resolution of seven grid cells in the half-width of the horseshoe region for all the computations in the interval 20–70 Earth masses. We have checked that this is needed in order to have results independent of the resolution. For small planetary masses a resolution of four grid cells is enough to achieve convergence (see Table 2).

In Fig. 5 (top) we report the total torque computed on planets held on fixed orbits at 4 au. The transition from inwards to outwards migration of small masses occurs for planet masses about twice as big as predicted by the Paardekooper et al. formula. We find again the 'cold finger' effects, with a transition to negative torque at about 10 Earth masses.

In the interval $[15, 30]\,M_\oplus$ we observe a positive total torque with values smaller than expected from the formula as in the previously examined RED and SED. In the interval $[40, 70]\,M_\oplus$ the results from numerical simulations very nicely agree with the torque provided by the analytical formula. We find positive torques up to planetary masses of $60\,M_\oplus$.

Similar results are found at 5 au and 6 au (Fig. 5, middle and bottom panels); precisely, cores of $50\,M_\oplus$ undergo outwards migration at 5 au and at 6 au. From the migration map the transition between outwards and inwards migration occurs for slightly larger masses; however the overall picture and the radial extent of the outwards migration are quite well reproduced.

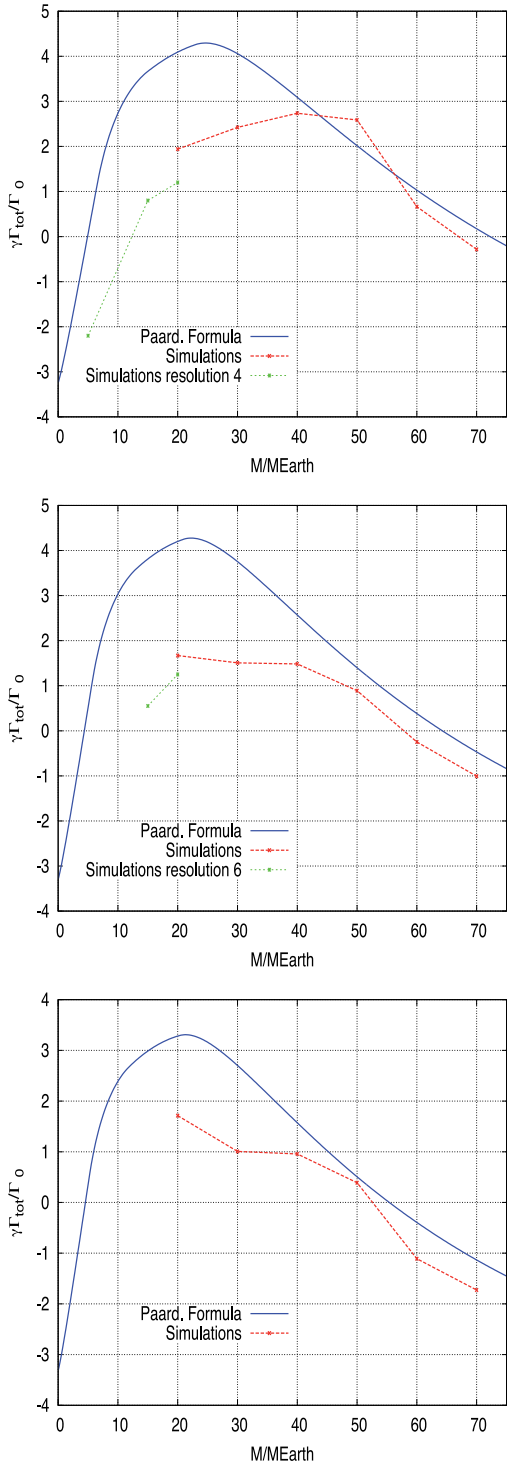

Figure 5. Accretion disc: comparison with Paardekooper et al. (2011) formula. Top panel: planets at 4 au; middle: planets at 5 au; bottom panel: planets at 6 au. The red points are obtained with a resolution of seven grid cells in the half-width of the horseshoe region, the green ones with a resolution of four grid cells.

As we pointed out in Section 3 this is an important result for models of giant planet formation. This may solve the problem pointed out in Coleman & Nelson (2014) where all planets were lost by migration before becoming gas-giant planets. However, we stress that this is true only for discs with large $\dot{M}$ like the one studied here.

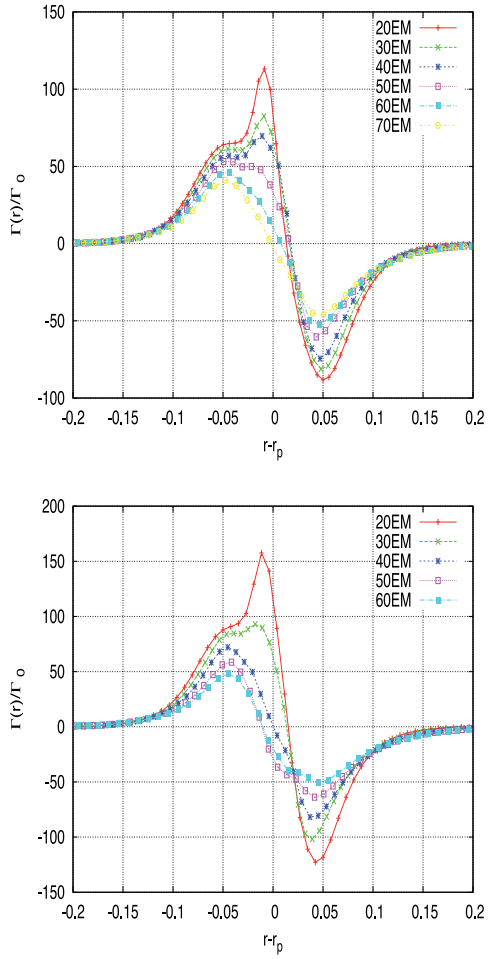

Figure 6. Radial torque density for planets of different masses at 5 au in the accretion disc with $\dot{M} = 4 \times 10^{-8}\,\mathrm{M}_{\odot}\,\mathrm{yr}^{-1}$ (top) and in the RED disc for planets at 5.2 au (bottom).

As pointed out in Bitsch et al. (2014, 2015), the maximum planet mass for outwards migration decreases with decreasing $\dot{M}$.

5.1 Radial torque distribution

To further confirm that the outwards migration detected in the accretion disc corresponds to that previously found in radiative discs without stellar heating and without a net mass flux through the disc we show the contribution to the torque in the close vicinity of the planets for both SAD and RED. We compute the radial torque density $\Gamma(r)$, i.e. the torque exerted on the planet by a ring of disc material located at a distance r from the star. The integral of $\Gamma(r)$ on the radial coordinate provides the total torque $\Gamma_{\rm tot}$ shown in the previous section:

$$\Gamma_{\rm tot} = \int_{r_{\rm min}}^{r_{\rm max}} \Gamma(r)\mathrm{d}r \ . \tag{8}$$

Fig. 6 shows the radial distribution of the torque exerted on planets of different masses in the accretion disc with $\dot{M} = 4 \times 10^{-8}\,\mathrm{M}_{\odot}\,\mathrm{yr}^{-1}$ at 5 au (top panel) and the radial torque density for the RED disc for planets placed at 5.2 au (bottom panel).

In a disc without thermal effects (isothermal disc) $\Gamma(r)$ would be positive for $r < r_{\rm p}$ and negative for $r > r_{\rm p}$. Moreover, $\Gamma(r)/\Gamma_0$ would be independent of the planet's mass. Here we observe that $\Gamma(r)/\Gamma_0$ changes with the planetary mass. This effect is due to the saturation of the entropy-driven corotation torque (Baruteau & Masset 2008; Kley et al. 2009) which is a function of planetary masses. We remark in Fig. 6 that, when the planetary mass increases from 20 to 70 $\mathrm{M}_{\oplus}$, the absolute value of Γ/Γ_0 decreases and the location where Γ transits from positive to negative, which is at $r > r_{\rm p}$ for the 20 $\mathrm{M}_{\oplus}$ planet, approaches $r_{\rm p}$. The displacement of the point where $\Gamma(r) = 0$ relative to $r_{\rm p}$ is indicative of the strength of the total positive torque. In this case, the total torque decreases for increasing planetary mass, until it becomes slightly negative for the 70 $\mathrm{M}_{\oplus}$ planet. In the case of the RED disc the results are very similar, although one can notice quantitative differences. In this case, $\Gamma(r_{\rm p}) = 0$ for a planet of 40 $\mathrm{M}_{\oplus}$. In fact, the transition to inwards migration occurs at about 40 $\mathrm{M}_{\oplus}$, as shown in Fig. 4.

6 ON THE WIDTH OF THE HORSESHOE REGION

We now go beyond the raw comparison of the torques predicted in Paardekooper et al. formula and measured numerically, in order to understand how such a good agreement is achieved for large masses but not for low masses. This is indeed surprising because the formula is derived in principle in the linear regime, while for $m_{\rm p} > 30\,\mathrm{M}_{\oplus}$, where the agreement is best, the non-linearities should start to appear (because of the condition $q > h^3$). Here we focus on the size of the corotation zone, which is a key parameter for the estimate of the corotation torque and of the torque saturation.

According to Masset et al. (2006) equation (3), obtained for 2D discs, is valid only for planet to star mass ratio $q < h^3$. The horseshoe region for large masses [$q > 1.5 \times 10^{-4}$ in Masset et al. (2006)] behaves as in the restricted three-body problem (RTBP), i.e. scales with $q^{1/3}$. For intermediate masses, the width of the horseshoe region is larger than that predicted by the $q^{1/2}$ scaling. This is a manifestation of the flow non-linearity turning out in a boost of the corotation torque (Masset et al. 2006).

In this section, we provide a measure of the half-width of the horseshoe region ($x_{\rm hs3D}$ hereafter), for SED and for the SAD with planets, respectively, at 4 au and at 5 au and compare it to $x_{\rm hs2D}$ of equation (3). Since differences with respect to equation (3) can come from 3D effects as well as from radiative effects we will proceed in two steps: (i) we determine the difference between the horseshoe width in 2D and 3D simulations in an isothermal setting, (ii) we compare isothermal 3D to fully radiative 3D.

6.1 Comparison between 2D and 3D simulations

For the 2D case we used the FARGO code (Masset 2000). We recall that in 2D a softening length ϵ is applied to the planet potential through:

$$\Phi = -\frac{Gm_{\rm p}}{\sqrt{a_{\rm p}^2 + \epsilon^2}}. \tag{9}$$

In 2D models, equation (9) allows to mimic the average influence that the planet would have on the vertical gas column. The measure of the width of the horseshoe region is determined by computing the streamlines. In Fig. 7 we plot the half-width of the horseshoe region normalized over the planet semi-major axis $a_{\rm p}$ for different values of the planet to star mass ratio q in the mass range considered in this paper ([10, 70] $\mathrm{M}_{\oplus}$). Using the nominal setting given in Masset et al. (2006) we recover their results (see their fig. 9). In Fig. 7 the

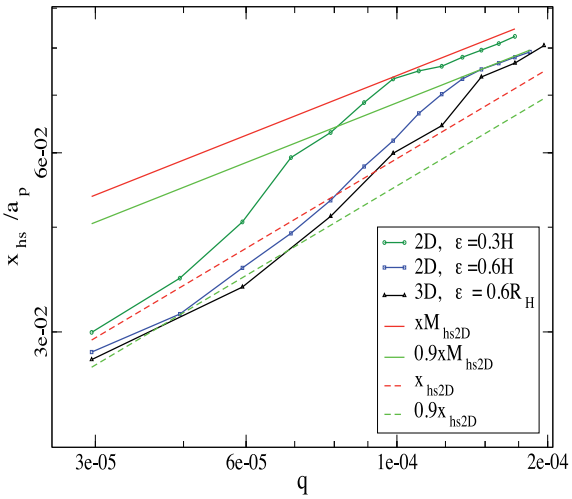

Figure 7. Simulations with isothermal EOS. Half-width of the horseshoe region normalized over a_p as a function of the planet to star mass ratio q. Results are shown for two sets of 2D simulations with respectively $\epsilon = 0.3H$ and $\epsilon = 0.6H$ and for 3D simulation with isothermal equation of state and $\epsilon = 0.6R_H$. The lines show the different fits in $q^{1/2}$(with labels x_{hs2D} and $0.9x_{hs2D}$, see text) and $q^{1/3}$ (with labels xM_{hs2D} and $0.9xM_{hs2D}$, see text).

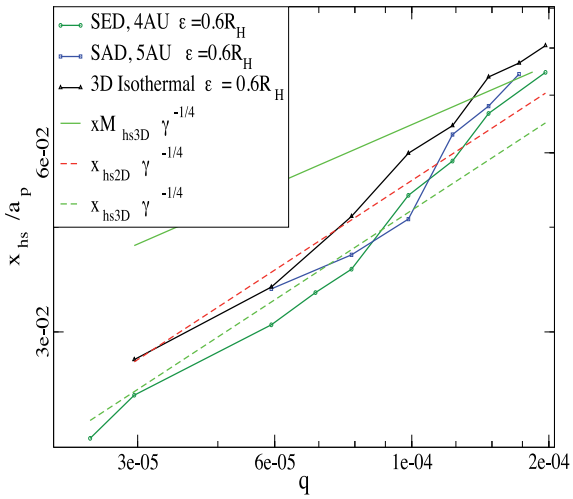

Figure 8. Same as Fig. 7 for 3D simulations for respectively SED with planets at 4 au, and SAD with planets at 5 au and for the 3D isothermal run of Fig. 7. The lines show the fits in $q^{1/2}$ and $q^{1/3}$. The law for the horseshoe region used in the Paardekooper formula, $x_{hs2D}\gamma^{-1/4}$, is also shown.

half-width of the horseshoe region obtained with a softening length of $\epsilon = 0.3H$ (as in Masset et al. 2006) is fitted by

$$x M_{hs2D} \simeq 2.45a(q/3)^{1/3} \quad (10)$$

for $q > 1.35 \times 10^{-4}$ while the x_{hs2D} law of equation (3) nicely fits the data for $q \leq 4.5 \times 10^{-5}$. The value of the aspect ratio for these simulations is $h = 0.044$; this value is used in the plot of the x_{hs2D} law.

We remark that in 2D the effect of the softening is felt well outside the Hill radius, so that the horseshoe region clearly depends on the softening length. In all our 3D numerical simulations we have used a softening length of $0.6R_H$. In order to compare 2D and 3D isothermal results we have also run a set of 2D simulations with a softening length of $\epsilon = 0.6H$. In Fig. 7 we observe that in this case the transition between the $q^{1/2}$ and the $q^{1/3}$ scaling occurs in the mass interval $9 \times 10^{-5} < q < 1.65 \times 10^{-4}$. The width of the horseshoe region, both in the linear and in the RTBP regime, is reduced by about 10 per cent with respect to the values obtained for the smaller softening length. In Fig. 7 we have also reported the measure of the width of the horseshoe region obtained with 3D isothermal simulations with $\epsilon = 0.6R_H$. The disc parameters are the ones of SAD set, with planets at 5 au. The aspect ratio at this distance from the star is $h = 0.044$ (Fig. 1). For 3D simulations the measure of the width of the horseshoe region is determined by computing the streamlines on the disc mid-plane. Results are in good agreement with the 2D case with $\epsilon = 0.6H$[5] so that we do not observe 2D versus 3D effects in the horseshoe region width.

6.2 Comparison between 3D isothermal and 3D radiative simulations

We call $xM_{hs3D} \simeq 0.9xM_{hs2D}$ the width of the horseshoe region obtained by the fit of 3D isothermal simulations in the RTBP regime and $x_{hs3D} \simeq 0.9x_{hs2D}$ the fit obtained for the linear regime. Fig. 8 shows the measure of the width of horseshoe region for SED with planets at 4 au,[6] and SAD with planets at 5 au.

For comparison we plot the results of the 3D isothermal simulations of Fig. 7. We recover a regime with a $q^{1/2}$ scaling and a regime with a $q^{1/3}$ scaling and in both regimes the horseshoe region is narrower than in the isothermal case of about a factor $\gamma^{-1/4}$ as expected from Paardekooper & Papaloizou (2009). In the same Fig. 8 we have plotted the law for the horseshoe region used in the Paardekooper formula, i.e. $x_{hs2D}\gamma^{-1/4}$.

We observe that the measured horseshoe width is respectively $\simeq$ 10 per cent narrower than $x_{hs2D}\gamma^{-1/4}$ in the linear (or $q^{1/2}$ scaling) regime and about $\simeq$ 10 per cent larger in the non-linear (or $q^{1/3}$ scaling) regime. Now a larger horseshoe region causes saturation earlier. We discuss this point in Section 6.4.

In the isothermal case the transition between the two regimes is associated with a boost in the corotation torque (Masset et al. 2006) and a small softening length is required to detect it. Therefore, we can wonder if we have missed some effects in the torque computation by using a softening length of $0.6R_H$.

6.3 Comparison between 3D radiative discs with different softening length

In the case of 3D isothermal simulations it has been shown (Kley et al. 2009) that a decrease in the softening length for a planet of 20 $M_\oplus$ corresponds to a drastic change in the density structure in the planet vicinity which has an important impact on the corotation torque. Precisely, the authors found a torque excess in agreement with Masset et al. (2006). The situation changes when taking into account thermal effects. In this case a deeper potential corresponds to an increase of temperature near the planet so that the density distribution close to the planet is not drastically changed. In Kley et al. (2009) (their fig. 14, top) changing the smoothing length from $\epsilon = 0.8R_H$ and $\epsilon = 0.5R_H$ in a fully radiative setting acts in increasing the torque of about 5 per cent, with respect to 30 per cent

[5] A value of the softening length of $\epsilon = 0.7H$ is shown to provide a radial torque density very similar to the one obtained with 3D simulations (see Kley et al. 2012.)

[6] The aspect ratio for SED at 4 au is $\tilde{h} = 0.041$ (Fig. 1). To be compared to the other data sets having $h = 0.044$ a rescaling by $\sqrt{\tilde{h}/h}$ is applied.

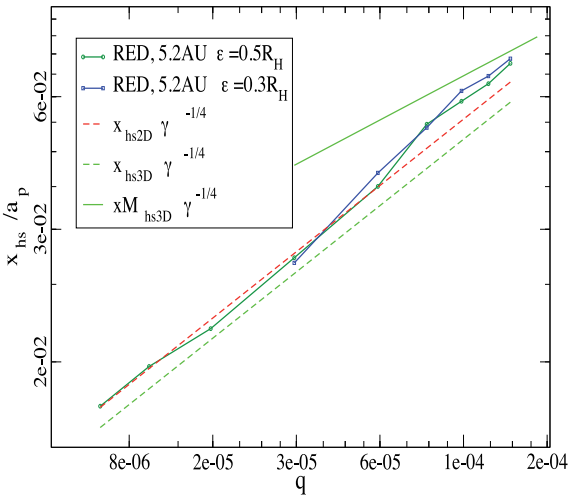

Figure 9. Half-width of the horseshoe region as a function planet to star mass ratio (q) for 3D simulations of RED set, for respectively $\epsilon = 0.5R_{\rm H}$ and $\epsilon = 0.3R_{\rm H}$. The lines show the fits in $q^{1/2}$ and $q^{1/3}$ obtained for the stellar irradiated discs (Fig. 8). The law for the horseshoe region used in the Paardekooper formula, $x_{\rm hs2D}\gamma^{-1/4}$, is also shown.

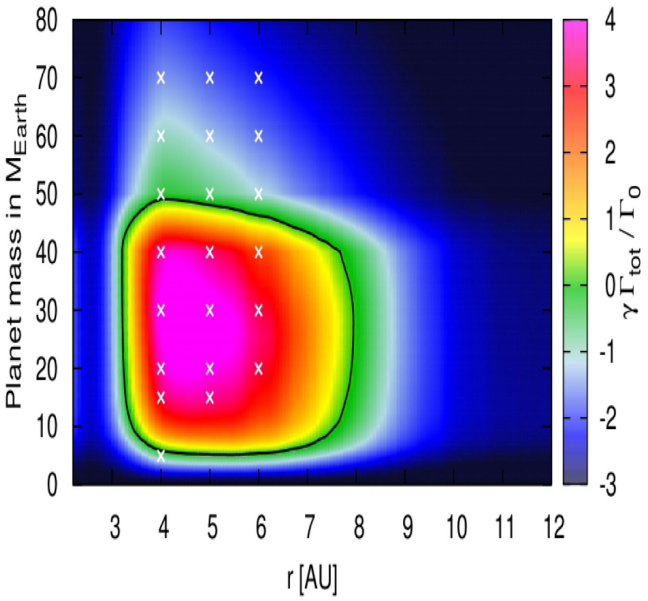

Figure 10. Migration maps for simulation set SAD with $\dot{M} = 4 \times 10^{-8}\,{\rm M}_\odot\,{\rm yr}^{-1}$ obtained using the width of the horseshoe region measured by our simulations (Fig. 8) instead of $x_{\rm hs2D}\gamma^{-1/4}$.

of increase in the corresponding isothermal case. We have extended the discussion of Kley et al. (2009) concerning the dependence of the torque on the softening length by computing the width of the horseshoe region and the total torque acting on fixed planets in the range [10: 60] $\rm M_\oplus$ for the RED set with $\epsilon = 0.3R_{\rm H}$. In Fig. 9 it appears clearly that the width of the horseshoe region is almost not affected by the change in the softening length.[7] The measured torque is also almost not affected by the change in the softening length.

We observe that in the $q^{1/2}$ regime the horseshoe region is nicely fitted by the law used in the Paardekooper formula (Fig. 9). However, although the measured width of the horseshoe region perfectly matches the law used in the formula up to 20 $\rm M_\oplus$ the measured torque fits only qualitatively the one provided by the formula as explained in Section 4.2. This is not surprising since many other parameters enter in the formula and can possibly be different in realistic 3D discs.

In isothermal discs a torque excess is correlated to the departure from the linear regime (Masset et al. 2006) while in all our radiative discs we do not observe the same phenomenon. Taking into account thermal effects, the transition from the linear to the non-linear regime, even considering a small softening length (Fig. 9), is smoother in radiative discs (Figs 8 and 9) with respect the isothermal case with small softening length (Fig. 7). Moreover, the mass at which we observe a departure from the linear regime in Figs 8 and 9 corresponds to the onset of torque saturation in Figs 3, 4 and 5 (middle panel).

6.4 Impact of the measured horseshoe width on planet migration

The width of the horseshoe region is of crucial importance for the saturation of the torque acting on more massive planets. A larger width of the horseshoe region increases the viscous time-scale (equation 6) making torque saturation easier. As demonstrated in Figs 8 and 9, the width of the horseshoe region increases for more massive planets and does not follow the simple law of $x_{\rm hs2D}\gamma^{-1/4}$, which is only valid for low-mass planets.

In Fig. 10 we show the migration map of the SAD disc, where we used the width of the horseshoe region measured by our simulations (Fig. 8) instead of $x_{\rm hs2D}\gamma^{-1/4}$. When comparing to Fig. 2, top panel, we see that for planetary masses of up to 40 $\rm M_\oplus$ the migration map remains unchanged while for larger planetary masses, we observe that the transition of the torque from positive to negative occurs in the interval 40–50 $\rm M_\oplus$. The transition occurs in the interval 60–70 $\rm M_\oplus$ in Fig. 2 (top panel). This is caused by a larger width of the horseshoe region, which makes saturation of the corotation torque easier. Hence the total torque transitions into negative values at smaller planetary masses. Adapting the width of the horseshoe region to our measured values in the torque formula therefore overpredicts the transition to inward migration compared to our simulations.

The difference between our simulations and the torque predicted by the formula is therefore not only caused by a different width of the horseshoe region. The cooling process plays also an important role and the vertical cooling in 2D disc is treated like blackbody radiation, while our 3D disc features vertical heat diffusion.

Therefore we think that the quantitative agreement between the torque formula of Paardekooper et al. (2011) and simulations for planetary masses $m_{\rm P} > 30\,{\rm M}_\oplus$ is a coincidence and the formula should be updated with results of 3D simulations. However, this is beyond the scope of this paper and left for future work.

7 CONCLUSION

Using 3D hydrodynamical simulations including stellar and viscous heating as well as radiative cooling we have computed the torque acting on planets of various masses kept on fixed circular orbits in both equilibrium and accretional protoplanetary discs. We confirm the results previously obtained on constant viscosity equilibrium discs, where the only source of heating was provided by viscous friction. The comparison between the total torque obtained with

[7] The aspect ratio for RED at 5.2 au is $\tilde{h} = 0.04$ (Fig. 1). To be compared to data having $h = 0.044$ a rescaling by $\sqrt{\tilde{h}/h}$ is applied.

numerical simulations and the one predicted by semi-empirical formula (Paardekooper et al. 2011) is in quantitatively good agreement for large masses ($>20\,M_\oplus$). In particular, the formula predicts well the maximum planet mass at which inwards migration is prevented by the action of the entropy-driven corotation torque.

Instead, although our results remain similar to those expected by the Paardekooper formula, we observe quantitative differences as large as a factor of $\sim$2 concerning: (i) the value of the maximum positive torque as a function of the planet's mass, (ii) the value of the planet mass at which the torque is maximal and (iii) the minimum planet mass allowing outwards migration. The last difference is due to the presence of a 'cold finger effect' already discussed extensively in Lega et al. (2014). The differences concerning the items (i) and (ii) have already been pointed out by Kley et al. (2009) as caused by differences between 2D and 3D effects. Moreover, by measuring the width of the horseshoe region we have observed that the value of the planet mass at which the torque is maximal is correlated to the departure from the linear regime. For large planetary masses the quantitatively good agreement between the numerical results and the prediction of the analytic formula was unexpected since the formula is based on unperturbed discs while planets with masses larger than $20\,M_\oplus$ start opening a partial gap. Precisely, torque saturation has the same behaviour in the torque formula and in simulations though saturation effects appear for larger planetary masses with respect to the torque formula. From the measure of the width of the horseshoe region, we have found that the onset of saturation is correlated to the onset of the non-linear regime not taken into account by the formula. Plugging the measured horseshoe width in the formula gives a worse comparison. Therefore, we think that the quantitative agreement on large masses is a coincidence, and future works is needed to provide a more accurate torque expression.

At the present state of the art, though there are some differences between the torque formula and 3D simulations, the zero torque location at the transition from outwards to inwards migration at large planetary masses is reproduced surprisingly well, making the formula applicable to the study of planetary migration properties from the unperturbed disc structure.

ACKNOWLEDGEMENTS

We thank an anonymous referee for raising important points on the relation between the width of horseshoe region and the corotation torque. The Nice group is thankful to ANR for supporting the MOJO project (ANR-13-BS05-0003-01). This work was performed using HPC resources from GENCI [IDRIS] (Grant 2014, [100379]). BB thanks the Knut and Alice Wallenberg Foundation for their financial support.

REFERENCES

Baruteau C., Masset F., 2008, ApJ, 672, 1054
Bitsch B., Kley W., 2010, A&A, 523, A30
Bitsch B., Kley W., 2011, A&A, 536, A77
Bitsch B., Crida A., Morbidelli A., Kley W., Dobbs-Dixon I., 2013, A&A, 549, 124
Bitsch B., Morbidelli A., Lega E., Crida A., 2014, A&A, 564, A135
Bitsch B., Johansen A., Lambrechts M., Morbidelli A., 2015, A&A, 575, A28
Coleman G. A. L., Nelson R. P., 2014, MNRAS, 445, 479
Cossou C., Raymond S. N., Hersant F., Pierens A., 2014, A&A, 569, 56
Crida A., Baruteau C., Kley W., Masset F., 2009, A&A, 502, 679
Hartmann L., Calvet N., Gullbring E., D'Alessio P., 1998, ApJ, 495, 385
Kley W., Crida A., 2008, A&A, 487, L9
Kley W., Bitsch B., Klahr H., 2009, A&A, 506, 971
Kley W., Müller T. W. A., Kolb S. M., Benítez-Llambay P., Masset F., 2012, A&A, 546, 99
Lega E., Crida A., Bitsch B., Morbidelli A., 2014, MNRAS, 440, 683
Lynden-Bell D., Pringle J. E., 1974, MNRAS, 168, 603
Lyra W., Paardekooper S.-J., Mac Low M.-M., 2010, ApJ, 715, L68
Masset F. S., 2000, A&AS, 141, 165
Masset F. S., Casoli J., 2009, ApJ, 703, 857
Masset F. S., Casoli J., 2010, ApJ, 723, 1393
Masset F. S., D'Angelo G., Kley W., 2006, ApJ, 652, 730
Paardekooper S.-J., Mellema G., 2006, A&A, 459, L17
Paardekooper S.-J., Papaloizou J. C. B., 2009, MNRAS, 394, 2297
Paardekooper S.-J., Baruteau C., Crida A., Kley W., 2010, MNRAS, 401, 1950
Paardekooper S.-J., Baruteau C., Kley W., 2011, MNRAS, 410, 293
Shakura N. I., Sunyaev R. A., 1973, A&A, 24, 337

This paper has been typeset from a TEX/LATEX file prepared by the author.